Journal of Controlled Release 196 (2014) 370–383

Contents lists available at ScienceDirect

Journal of Controlled Release

journal homepage: www.elsevier.com/locate/jconrel

ROS-triggered and regenerating anticancer nanosystem: An effective strategy to subdue tumor's multidrug resistance

Zhigui Su [a], Minglei Chen [a], Yanyu Xiao [a], Minjie Sun [a], Li Zong [a,*], Sajid Asghar [a,c], Mei Dong [b], Huipeng Li [a], Qineng Ping [a,*], Can Zhang [a]

[a] State Key Laboratory of Natural Medicines, China Pharmaceutical University, 24 Tong Jia Xiang, Nanjing 210009, PR China
[b] Key Laboratory of Human Functional Genomics of Jiangsu Province, School of Basic Medical Science, Nanjing Medical University, 140 Hanzhong Road, Nanjing 210029, PR China
[c] College of Pharmacy, Government College University Faisalabad, Faisalabad, Pakistan

ARTICLE INFO

Article history:
Received 15 June 2014
Accepted 21 September 2014
Available online 30 September 2014

Keywords:
Tumor microenvironment
Reactive oxygen species
Targeted drug delivery nanosystem
Multidrug resistance
ROS-triggered and regenerating

ABSTRACT

Drug delivery strategies utilizing tumor microenvironment are recognized as a critical doorway to overcome multidrug resistance (MDR). However, the variability of tumor microenvironment at different disease stages would definitely minimize stimuli generation and eventually the therapeutic effects of these stimuli sensitive systems. Herein, we report a unique reactive oxygen species (ROS) triggered nanosystem that can replenish the ROS upon disassembly to maintain its high level. This was accomplished by a new amphiphilic polymer (TBH) composed of D-α-tocopherol polyethylene glycol 1000 succinate (TPGS), hyaluronic acid (HA) and arylboronic ester. As a linker of TPGS to HA, arylboronic ester could efficiently degrade in response to ROS resulting in dismantling of nanosystem followed by rapid release of TPGS. Owing to ROS inducing activity of TPGS with mitochondrial respiratory complex II, ROS regeneration was observed for TBH nanosystem both in MCF-7/ADR cells and tumor tissues xenografted with MCF-7/ADR cells. Furthermore, doxorubicin-loaded TBH nanosystem (DOX-TBH) revealed higher drug cytotoxicity due to enhanced retention effect on account of ROS triggered DOX release and P-gp inhibitory mechanism of TPGS. Moreover, HA significantly improved tumor targeting capability of DOX-TBH, while ROS based triggering and regenerating mechanism lead to marked inhibition of the tumor growth in the xenograft MCF-7/ADR tumor-bearing nude mice.

1. Introduction

Cancer, one of the most challenging and complex global maladies, is affecting the life of people around the world. Despite multiple anticancer strategies have been used, chemotherapy continues to be an important therapeutic option for different malignancies, especially for primary advanced and metastatic tumors. However, the efficacy of chemotherapy is substantially limited by the intrinsic and acquired resistance of cancer cells to the anticancer drugs, which contributes to therapeutic failure and tumor relapses in over 90% of patients [1]. Multidrug resistance (MDR) in cancer cells is a complex phenomenon that may result from numerous mechanisms. The overexpression of pumps of the ATP-binding cassette superfamily (ABCs) present within the cancer cell membrane is one of the most well-known mechanisms, leading to reduced drug uptake. This requires excessive drug doses to kill tumor cells but that can induce severe adverse side effects on healthy tissues [2,3].

With the advancement of drug delivery technologies, a series of new drug delivery systems (DDS) has been developed to provide many alternative strategies to circumvent MDR based on overexpression of ABCs. But, the poor cellular uptake and insufficient intracellular drug release remain rate-limiting steps in reaching the drug concentration level within the therapeutic window [4]. Therefore, a site-dependent drug release character triggered by intracellular pH [5,6], redox property [7] or enzyme levels [8,9] could be vital to obtain a sufficiently high intracellular level of drugs for overcoming MDR. Recently, one of the most popular approaches is to target redox property of cancer cells, utilizing disulfide or thiolysis bonds as triggered linkers owing to their tendency to be cleaved by elevated intracellular glutathione (GSH) [10–13]. However, redox property of cancer cells is a dynamic milieu [14], because cancer cells frequently develop multiple genetic alterations. Redox property changes during cancer development and disease progression, even one tumor cell at different stages may have different redox signal levels [15]. To counter the varying stimuli level, some studies designed the nanocarriers by using double stimuli responsive strategy: sensitive to both GSH and ROS [16] or GSH and pH [17]. Therefore, a delivery system that aims to amplify levels of triggered signal to satisfy the signal response needs would have important implications for potential anticancer therapeutics. Xiong et al. revealed that a lipase-sensitive polymeric nanogel selectively degraded through fabrication of a special lipase accumulated tumor environment [18]. Maltzahn et al. constructed the

* Corresponding authors. Tel./fax: +86 25 83271092.
E-mail addresses: zongcpu@126.com.cn (L. Zong), pingqn@cpu.edu.cn (Q. Ping).

http://dx.doi.org/10.1016/j.jconrel.2014.09.020
0168-3659/

communicating nanoparticle systems composed of signaling and receiving modules that activate the coagulation cascade in target tumors [19]. Inspired by the fact that magnifying diseased tissue signal could significantly improve targeting in biological systems in vivo, we speculate that constructing a constant high level of ROS in cytoplasm as amplifying signaling modules would facilitate the action of ROS signal sensitive nanocarriers.

Herein, we report a novel ROS triggering and positive feedback nanosystem assembled from a new amphiphilic polymer composed of D-α-tocopherol polyethylene glycol 1000 succinate (TPGS), hyaluronic acid (HA) and arylboronic esters to effectively overcome multidrug resistance. As shown in Fig. 1, to achieve a positive feedback ROS signal in cytoplasm, we selected α-tocopheryl polyethylene glycol succinate (TPGS), a polyethylene glycol (PEG) conjugate of α-tocopheryl succinate (α-TOS). TPGS is not only an effective P-gp efflux inhibitor [20] and selective cancer cell killing agent [21], but is also a powerful ROS inducer upon its interaction with mitochondrial respiratory complex II [22,23]. In addition, the arylboronic ester was chosen as ROS sensing linker because of its facile ROS mediated degradation at physiological pH and temperature, which has been studied for imaging and targeting of tumor cells [24]. Amphiphilic material (TBH) was prepared by linking hyaluronic acid (HA) as hydrophilic chains to the hydrophobic TPGS via arylboronic esters. Besides its biocompatibility, biodegradability and ease of modifications [25], HA is an active target ligand for CD44 positive malignant cells [26], which would be beneficial to increase the nanocarrier uptake.

As displayed in Scheme 1, to check the effectiveness of the nanosystem, doxorubicin (DOX) as an anticancer agent that is resisted by cancer cells was loaded in TBH micelles (DOX-TBH). After CD44 mediated endocytosis, the arylboronic ester in DOX-TBH was expected to be triggered by intracellular ROS leading to the disassembly of DOX-TBH and burst release of TPGS and DOX. Upon interaction with mitochondrial respiratory complex II, TPGS induces the generation of ROS which may create a kind of ROS positive feedback microenvironment with persisting high levels of ROS generation necessary for degradation of TBH. In addition, TPGS acts as a P-gp inhibitor to hinder the efflux of DOX, which might ensure high intracellular levels of drugs, sufficient for overcoming MDR and inducing programmed cell death.

2. Materials and methods

2.1. Materials

D-α-Tocopherol polyethylene glycol 1000 succinate (TPGS) and DCFH-DA were purchased from Sigma-Aldrich Co. LLC. (Shanghai, China). DCFH-DA Reactive Oxygen Species Assay Kit, DiO, DiI, and Annexin V-FITC/PI Apoptosis Detection Kit were purchased from Beyotime Institute of Biotechnology Co. LLC. (Nantong, China). Hyaluronic acid (molecular weights 100 kDa) was purchased from Freda Biochem Co., Ltd. (Shandong, China). Doxorubicin HCl (DOX) was purchased from Internet Aladdin Reagent Database Inc. (Shanghai, China). DMEM (Hyclone®), fetal bovine serum (FBS, Hyclone®), penicillin–streptomycin solution (Hyclone®), trypsin (Hyclone®), phosphate buffered saline (PBS, Hyclone®) and MTT were provided by Sunshine Biotechnology Co., Ltd. (Nanjing, China). All other chemicals and reagents were HPLC or analytical grade.

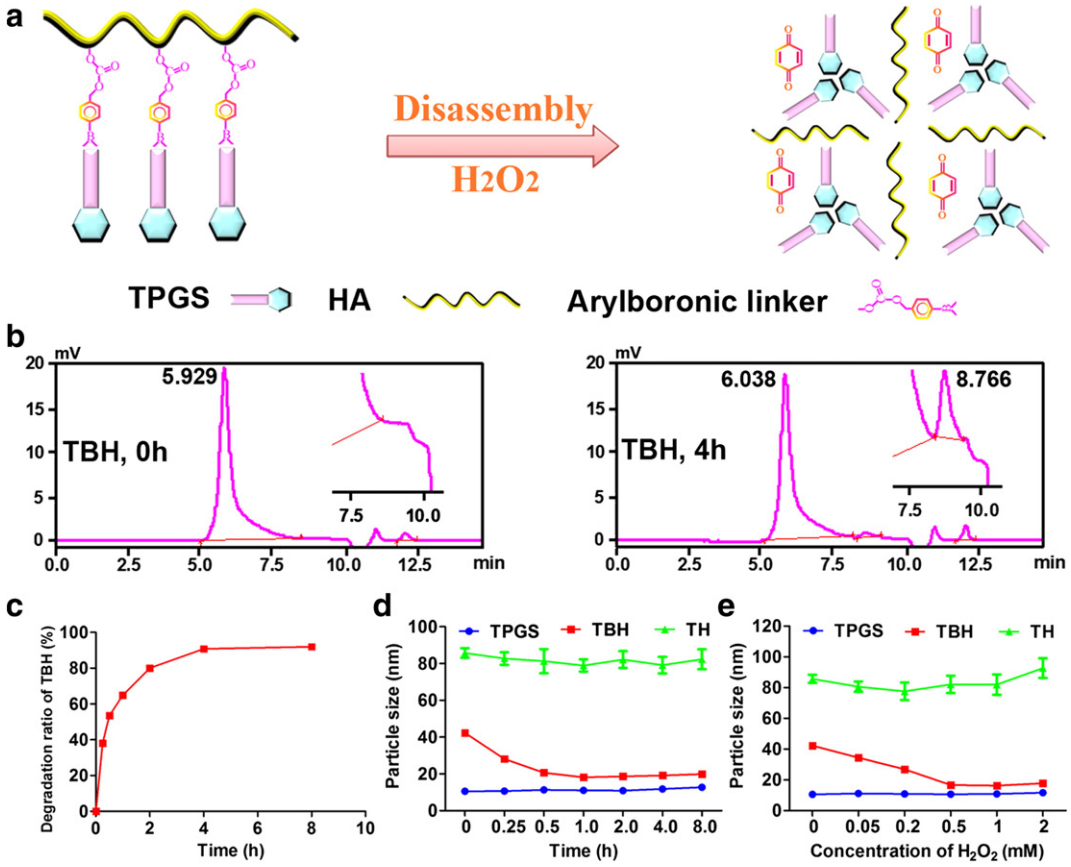

Fig. 1. ROS-triggered degradation of TBH. (a) Scheme of TBH disassembly under H_2O_2. (b) The GPC image of TBH at different times when incubated with 1 mM H_2O_2. (c) The degradation ratio of TBH in time course with 1 mM H_2O_2. (d) The change of particle size of TPGS, TBH and TH in different incubation times with 1 mM H_2O_2. (e) The change of particle size of TPGS, TBH and TH in the presence of different concentrations of H_2O_2 after 4 h of incubation.

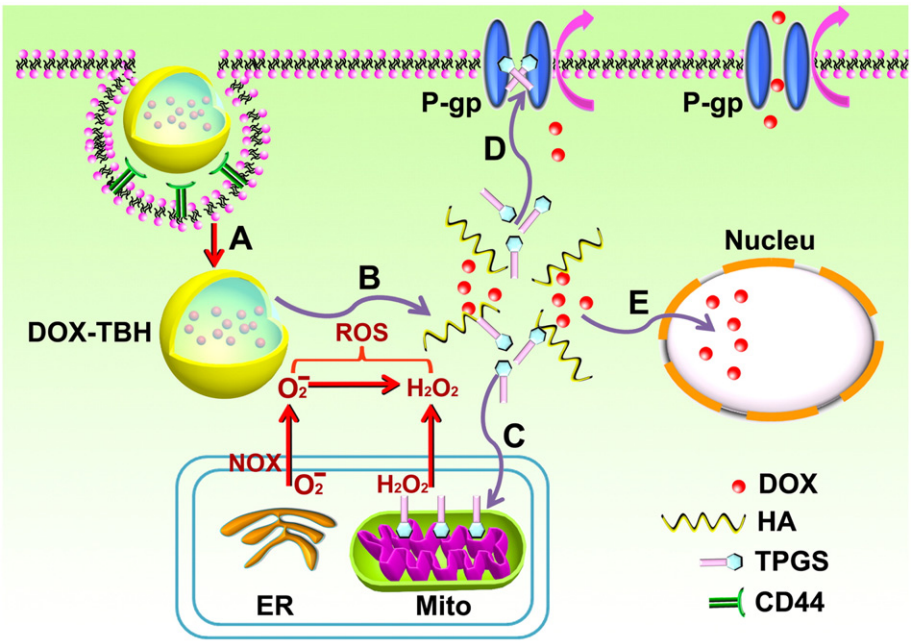

Scheme 1. The schematic presentation of ROS-triggered and regenerating anticancer nanosystem. A: TBH self-assembling nanosystem (DOX-TBH) and endocytosis mediated by HA through the overexpressed CD44 receptors; B: the breakage of arylboronic linkers by ROS, followed by DOX-TBH rapid disassembly and released DOX and TPGS; C: By acting on mitochondrial respiratory complex II, the released TPGS induced ROS generation for complete disassembly of DOX-TBH; D: TPGS as the inhibitor of P-gp efflux to overcome MDR; E: DOX as well as ROS induced cell death in nucleus.

2.2. Cell culture

P-gp overexpressing and DOX-resistant human breast adenocarcinoma cells (MCF-7/ADR) were used for the cell studies. MCF-7/ADR were cultured in DMEM medium, supplemented with 10% FBS, 100 U/mL of penicillin and 100 μg/mL of streptomycin at 37 °C using a humidified 5% CO_2 incubator.

2.3. Animals

The female athymic nude mice were obtained from the Shanghai Silaike Laboratory Animal Limited Liability Company and housed on standard laboratory diet at an ambient temperature and humidity in air-conditioned chambers. All the animals were pathogen-free and allowed to access food and water freely. All animal experiments were conducted in full compliance with local, national, ethical and regulatory principles with the approval of the Institutional Animal Care and Use Committee at China Pharmaceutical University. To construct xenograft MCF-7/ADR tumor-bearing nude mice, approximately 10^7 of MCF-7/ADR cells were incubated subcutaneously in the flank region of female athymic nude mice. Tumor volume (V) was determined by measuring length (L) and width (W), and calculated as Eq. (1):

$$V = 1/2 \times L \times W^2. \quad (1)$$

2.4. Synthesis and characterization of TBH

The synthesis of TBH was described in the Supplementary data. For comparison, composed of HA and TPGS another amphiphilic polymer without ROS sensitivity was synthesized and named as TH.

Gel-permeation chromatography (GPC) was used to evaluate the degradation of TBH in 1 mM H_2O_2 at different incubation times. GPC was performed using a Shimadzu LC20A HPLC system (Kyoto, Japan), a refractive index detector (RID-10A, Shimadzu Co.), LC solution software (Shimadzu Co.), and a SB-803 HQ column (300 mm × 8 mm, Shodex, Shoko America, Inc, Japan). The mobile phase was 0.1 M sodium nitrate at a flow rate of 1 mL/min, and the analyses were performed at 40 °C. The injection volume was 20 μL. TBH was dissolved in deionized water with 1 mM H_2O_2. After 0.25, 0.5, 1, 2, 4 and 8 h incubation, 20 μL of different samples was withdrawn and analyzed by GPC. The content of degradation products of TPGS was calculated by the standard curve of TPGS. The degradation ratio of TBH was calculated as Eq. (2):

$$\textit{Dregadation ratio of TBH}(\%) = W_D / W_T \times 100\%. \quad (2)$$

where W_D was the content of degradation products of TPGS and W_T was the total content of TPGS which was determined by colorimetric method as described by Peracchia et al. [27]. In addition, after 4 h incubation TBH solution was ultra-filtered with a molecular weight cutoff 10 kDa and then the ultrafiltrate was lyophilized and analyzed by ^{1}H NMR in $CDCl_3$. For comparison, HA, TPGS, mixture of HA and TPGS or TH was also analyzed by GPC.

Next, the dynamic light scattering (DLS) was also utilized to monitor the change of particle size when TPGS, TBH and TH were treated with H_2O_2. To evaluate time-dependent ROS degradation, TPGS, TBH and TH solution were firstly mixed with H_2O_2 in which the concentration of H_2O_2 was fixed at 1 mM and incubated for 0.25, 0.5, 1, 2, 4 and 8 h. To investigate concentration-dependent ROS degradation, TPGS, TBH and TH solution were incubated with different concentrations of H_2O_2 in a range of 0, 0.05, 0.2, 0.5, 1 and 2 mM for 4 h. After incubation, 3 mL of TPGS, TBH and TH solution was withdrawn and particle size was monitored with DLS (Brookhaven Instruments-ZetaPlus, USA).

2.5. Intracellular ROS detection

ROS generation inside cells was detected using DCFH-DA Reactive Oxygen Species Assay Kit. For quantitative evaluation of ROS generation efficacy, MCF-7/ADR cells were seeded in 24-well plates at a density of 105 cells/well and incubated for 24 h. Then, the medium was removed and the cells were treated with HBSS for 20 min. To investigate the effect of time-dependent ROS generation, cells were incubated with 200 μL of TPGS, TBH or TH solution and 200 μL of DMEM without FBS in which the concentration of TPGS was fixed at 200 μg/mL for 0.5, 1,

2, 3, 4 and 8 h at 37 °C. To investigate the effect of concentration-dependent ROS generation, the medium was replaced with 200 μL of TPGS, TBH or TH solution and 200 μL of DMEM without FBS in which the concentration of TPGS was in the range of 10, 20, 50, 100 and 200 μg/mL, and incubated for 4 h at 37 °C. At the end of the incubation period, the supernatant was removed and the wells were washed three times with ice-cold PBS. After treatment with DCFH-DA for 30 min, the cells were washed three times with ice-cold PBS, harvested and resuspended in PBS. The fluorescence was measured by flow cytometry (FACS-Calibur, BD Biosciences).

For qualitative analysis of ROS generation efficacy, MCF-7/ADR cells were seeded in confocal dishes at a density of 3 × 105 cells/dish. Following incubation with TPGS, TBH and TH (200 μg/mL calculated by TPGS) for 4 h, DCFH-DA was loaded into the cells. After 30 min incubation, cells were washed three times with ice-cold PBS and fluorescence images of treated cells were acquired using Confocal Laser Scanning Microscopy (CLSM) (Olympus FV1100, Japan).

2.6. Measurement of mitochondrial respiratory complex II activity

MCF-7/ADR cells were seeded in 24-well plates at a density of 10^5 cells/well. Following incubation with TPGS, TBH and TH (200 μg/mL calculated by TPGS) for different times (0, 0.5, 1, 2, 4 and 8 h), at the end of the incubation period the supernatant was removed and the wells were washed three times with ice-cold PBS. Subsequently, the cells were incubated with 200 μL of ice-cold cell lysis buffer for 10 min. Then, samples were centrifuged to remove the cellular debris at 4 °C. 20 μL aliquot of each cell lysate was used to determine the cell protein content using BCA Protein Assay Kit. The activity of mitochondrial respiratory complex II was measured according to the Mitochondrial Complex II Activity Assay Kit (Germany, Novagen). The relative activity of mitochondrial respiratory complex II was calculated by the Eq. (2):

$$\textit{Relative activity}(\%) = A_{(t)}/A_{(c)} \times 100\%. \quad (2)$$

where $A_{(t)}$ is the activity of mitochondrial respiratory complex II at different times and $A_{(c)}$ is the activity of mitochondrial respiratory complex II before incubation.

2.7. Ex vivo imaging studies for ROS generation in xenograft MCF-7/ADR tumor-bearing nude mice

When the tumor volume reached 0.2–0.3 cm^3, mice were first injected with free DCFH-DA (2.5 mg/kg) by intratumoral injection, then intravenous injection of saline as control, TPGS, TBH or TH at a dose of 50 mg of TPGS/kg. Mice were anesthetized using intraperitoneal injection of chloral hydrate (10 mg/kg). Ex vivo fluorescence imaging experiments were performed at 1, 4, 8, 12 and 24 h post-injection utilizing a Kodak multimodal-imaging system IS2000MM (Kodak, USA) equipped with an excitation bandpass filter at 460 nm and an emission at 535 nm. Exposure time was 30 s per image. Images were analyzed by Carestream Molecular Imaging Software V 5.3.5 (Kodak ID Image Analysis Software; Kodak). To confirm the biodistribution of DCFH-DA probes in different organs, the mice were sacrificed at 24 h post-injection. Different organs were separated and washed by saline and assembled for ex vivo fluorescence imaging. In addition, the tumor samples underwent frozen section examination with 7 μm thickness, stained with DAPI and observed by CLSM.

2.8. Preparation and characteristics of DOX-TBH and DOX-TH

DOX base was obtained by the overnight reaction of DOX·HCl with double mol ratio of triethylamine in formamide. DOX loading TBH (DOX-TBH) and TH (DOX-TH) micelles were assembled in a simple dialysis technique. 40 mg TBH or TH was dissolved in 2 mL of distilled water. 1 mL of DOX formamide solution (4 mg/mL) was added into the polymers solution under stirring for 1 h. The mixture solution was dialyzed against distilled water using a dialysis bag (MWCO of 3.5 kDa) for 24 h to remove free DOX. Dialyzed products were filtered through a 0.22 μm microfiltration membrane. Particle size, polydispersity index and zeta potential of DOX-TBH and DOX-TH were determined by Brookhaven Instruments-ZetaPlus (Brookhaven, USA). The morphological observations were performed under TEM (H-600, Hitachi, Japan) following negative staining with 0.1 wt.% sodium phosphotungstate solution. Particle degradation study was performed with 1 mM H_2O_2 to confirm oxidation sensitive characteristic.

The concentration of DOX in DOX-TH and DOX-TBH was determined by Shimadzu 10-A vp HPLC system (Kyoto, Japan). The stationary phase, Diamonsil C_{18} column (150 mm × 4.6 mm, 5 μm), was kept at 40 °C. The mobile phase consisted of 5 mM ammonium acetate (pH 3.5, 0.05% triethylamine): methanol (30:70) and was delivered at a rate of 1.0 mL/min. The injection volume was 20 μL and effluent was monitored by a fluorescence detector (Shimadzu, Japan) with excitation wavelength of 480 nm and emission wavelength of 550 nm. DOX-TBH and DOX-TH were filtrated through the 0.22 μm cellulose nitrate membrane. The 50 μL of DOX-TBH or DOX-TH was dissolved in a mixture with 250 μL formamide and 700 μL methanol, and then vortexed for 30 s and centrifuged at 12000 rpm for 10 min. The drug concentrations before dialysis and after filtration were determined. The encapsulation efficiency (EE) in DOX-TBH and DOX-TH was calculated as Eq. (3):

$$EE(\%) = (C_a \times V_a)/(C_b \times V_b) \times 100\% \quad (3)$$

where C_a is the concentration of the drug after filtration and V_a is the volume of DOX-TBH or DOX-TH solutions after filtration. C_b is the concentration of the drug before dialysis and V_b is the volume of DOX-TBH or DOX-TH solutions before dialysis.

2.9. In vitro drug release of DOX-TBH and DOX-TH

In vitro drug release of DOX-TBH and DOX-TH was analyzed by a membrane dialysis technique. In order to investigate ROS-triggered release the study of drug release in vitro was done in 0.9% saline with or without 1 mM H_2O_2. 1 mL of DOX-TBH or DOX-TH (containing 200 μg of DOX) was placed into a dialysis bag (MWCO of 3.5 kDa). Meanwhile, DOX solution was prepared as control. The dialysis bag was tightened and soaked in 50 mL of 0.9% saline with or without 1 mM H_2O_2. The experiments were carried out at 37 °C for 8 h in 3 replicates. At predetermined intervals, 1 mL of the dissolution medium was withdrawn and replaced with the same amount of pre-warmed fresh medium. The samples of the replicates were analyzed by HPLC. The concentration of H_2O_2 was also determined by the method of ferrous oxidation in xylenol orange (FOX) assay [28].

To investigate the influence of different concentrations of H_2O_2 in 0.9% saline on drug release, H_2O_2 was added into DOX-TBH and DOX-TH solution with different final concentrations of H_2O_2 (0, 0.05, 0.2, 0.5, 1 and 2 mM). Free DOX was obtained by ultrafiltration method with molecular weight cutoff 10 kDa. The ratio of drug release from DOX-TBH and DOX-TH was calculated as Eq. (4):

$$\textit{Drug release}(\%) = C_u/C_o \times 100\% \quad (4)$$

where C_u is the concentration of DOX in the ultrafiltrate and C_0 is the total concentration of DOX before ultrafiltration.

2.10. FRET analysis of TBH disassembly in vitro

Fluorescence resonance energy transfer (FRET) analysis was conducted as previously reported [29,30]. A FRET pair of hydrophobic dyes, DiO as donor and DiI as acceptor, was physically loaded into the micelles cores. To verify the occurrence or disappearance of FRET,

fluorescence spectra of DiO and DiI double loaded micelles diluted in deionized water or deionized water with 1 mM H_2O_2 were measured using a fluorospectrophotometer (Shimadzu, RF-5301, Japan) with the excitation at 484 nm and the emission scan from 400 nm to 700 nm. The FRET ratio (FR) was calculated as Eq. (5):

$$FR(\%) = IR/(IR + IG) \times 100\% \quad (5)$$

where *IR* and *IG* are fluorescence intensities at 565 nm and 501 nm, respectively. DiO and DiI double loaded TBH (FRET-TBH) and TH (FRET-TH) micelles were prepared by a simple dialysis technique. Briefly, 40 mg TBH or TH was dissolved in 2 mL of distilled water. DiO and DiI were dissolved in 1 mL DMSO and added into the polymer solution under stirring for 1 h. The mixture solution was dialyzed against distilled water using a dialysis bag (MWCO of 3.5 kDa) for 24 h. Dialyzed products were filtered through a 0.22 μm microfiltration membrane.

MCF-7/ADR cells were incubated with FRET-TBH and FRET-TH for 2 h at 37 °C and washed with ice-cold PBS, and then incubated with culture medium at 37 °C for an additional 2, 3 and 4 h. CLSM images were acquired with the excitation at 484 nm, and the emission between 555 nm and 655 nm for DiI detection, as well as the emission between 500 nm and 530 nm for DiO detection. The fluorescence intensity of the hold cells was analyzed by Leica Application Suite Advanced Fluorescence Version: 2.3.0 build 5131. The fluorescence intensity of DiO was named as IG while the fluorescence intensity of DiI was named as IR. The FR was calculated as described in Eq. (5).

2.11. Determination of the intracellular accumulation, retention of DOX

MCF-7/ADR cells were seeded in 24-well plates at a density of 10^5 cells/well and incubated for 24 h. Then, the medium was removed and the cells were treated with HBSS for 20 min. To investigate time-dependent uptake, cells were incubated with 200 μL of free DOX, DOX-TBH or DOX-TH suspension and 200 μL of DMEM without FBS in which the concentration of DOX was fixed at 10 μg/mL and incubated for 1, 2, 3 and 4 h at 37 °C. To investigate concentration-dependent uptake, the medium was replaced with 200 μL of free DOX, DOX-TBH or DOX-TH suspension and 200 μL of DMEM without FBS in which the concentration of DOX was in the range of 2–20 μg/mL and incubated for 4 h at 37 °C. At the end of the incubation period, the supernatant was removed and the wells were washed three times with ice-cold PBS. Subsequently, the cells were incubated with 200 μL of cell lysis buffer for 10 min. Then, samples were centrifuged to remove the cellular debris at 4 °C. 20 μL aliquot of each cell lysate was used to determine the cell protein content using BCA Protein Assay Kit. The concentration of DOX in cell lysate was determined by HPLC as described above. The uptake index (UI) was calculated as Eq. (6) [31]:

$$UI = C/P \quad (6)$$

where *C* is the concentration of DOX in cell lysate and *P* is the concentration of protein in cell lysate.

To determine the intracellular retention of DOX, MCF-7/ADR cells were cultured with either free DOX, DOX-TBH or DOX-TH for 4 h, washed with ice-cold PBS, and then incubated with culture medium at 37 °C for an additional 0.5, 1, 2 and 4 h. Cells were lysed and the concentrations of DOX in cell lysate were measured as described above. The intracellular retention ratio was calculated as Eq. (7):

$$\text{Relative residual amounts}(\%) = UI_{(t)}/UI_{(0)} \times 100\% \quad (7)$$

where $UI_{(t)}$ is the value of *UI* at different additional incubation times and $UI_{(0)}$ is the value of *UI* before additional incubation.

2.12. The cytotoxicity and apoptosis of free DOX, DOX-TBH and DOX-TH in MCF-7/ADR cells

MCF-7/ADR cells were seeded in 96-well plates at a density of 5×10^3 cells/well and incubated for 24 h. MCF-7/ADR cells were incubated with free DOX, DOX-TBH and DOX-TH containing the same concentration of DOX (0.2–20 μg/mL) for 24 h and cytotoxicity was measured with MTT assay. After incubation, 10 μL of MTT (5 mg/mL in pH 7.4 PBS) was added and incubated for another 4 h; the medium was then replaced with 150 μL DMSO. The UV absorbance intensity of cells was measured by Microplate Reader (Thermo Electron Corporation, USA) at 570 nm. Each point was performed in triplicates.

Apoptosis of MCF-7/ADR was detected using the Annexin V-FITC/PI Apoptosis Detection Kit, the cells were incubated with free DOX, DOX-TBH and DOX-TH containing the same concentration of DOX (5 μg/mL) for 12 h. The following procedures were performed in accordance with the manufacturers' protocols. Finally, apoptosis was analyzed by flow cytometry (FACS-Calibur, BD Biosciences).

2.13. CLSM Study for uptake of free DOX, DOX-TBH or DOX-TH

MCF-7/ADR cells were placed in the confocal dishes at a density of 3×10^5 cells/dish. After 24 h of cell attachment, 500 μL of free DOX, DOX-TBH or DOX-TH (containing 10 μg/mL DOX) was added in the culture medium and incubated for 2 h at 37 °C. After incubation, the cells were washed thrice by ice-cold PBS and stained with Hoechst 33342 for 30 min at 37 °C. Then, the cells were again washed three times with ice-cold PBS and observed by CLSM.

2.14. Ex vivo imaging studies for tumor target ability of TBH and TH micelles

To investigate in vivo dynamic distribution and tumor-targeting, DiR, a hydrophobic near infrared dye, was loaded into TBH and TH micelles (DiR-TBH and DiR-TH). The xenograft MCF-7/ADR tumor-bearing nude mice were intravenously administrated with DiR-TBH or DiR-TH (2.5 mg/kg) and anesthetized using intraperitoneal injection of chloral hydrate (10 mg/kg). Ex vivo fluorescence imaging experiments were performed as mentioned above except that the wavelength was fixed at 720 nm for excitation and 790 nm for emission. To confirm the biodistribution of DiR probes in different organs, the mice were sacrificed at 24 h post-injection. Different organs were separated and washed by saline, assembled for fluorescence imaging and analyzed by Carestream Molecular Imaging Software V 5.3.5. In addition, the tumor samples underwent frozen section examination with 7 μm thickness, stained with DAPI and observed by CLSM.

2.15. In vivo biodistribution, inhibition of xenograft MCF-7/ADR tumor growth and analysis of apoptosis by TUNEL histology for free DOX, DOX-TBH and DOX-TH

The xenograft MCF-7/ADR tumor-bearing nude mice were intravenously injected with the free DOX, DOX-TBH and DOX-TH at DOX dose of 2.5 mg/kg. At indicated times (0.5, 4, 12 and 24 h) after injection, blood samples were collected and mice were then sacrificed by cervical dislocation. Tissues were excised and lightly rinsed to remove any excess blood, weighed and stored at −20 °C until assay. The concentration of DOX in plasma and homogenized tissues was determined by HPLC.

For in vivo antitumor evaluation, the xenograft MCF-7/ADR tumor-bearing nude mice were weighed and randomly divided into four groups: 1) saline; 2) free DOX (2.5 mg/kg); 3) DOX-TBH (2.5 mg/kg); 4) DOX-TH (2.5 mg/kg). The different formulations were administrated via tail vein at days 0, 2, 4, 6 and 8. Tumor size was measured every other day. The survival time of 4 groups treated as above was also monitored. To evaluate the apoptotic response in tumor tissues, the terminal deoxynucleotidyl transferase (TdT)-mediated dUTP-digoxigenin

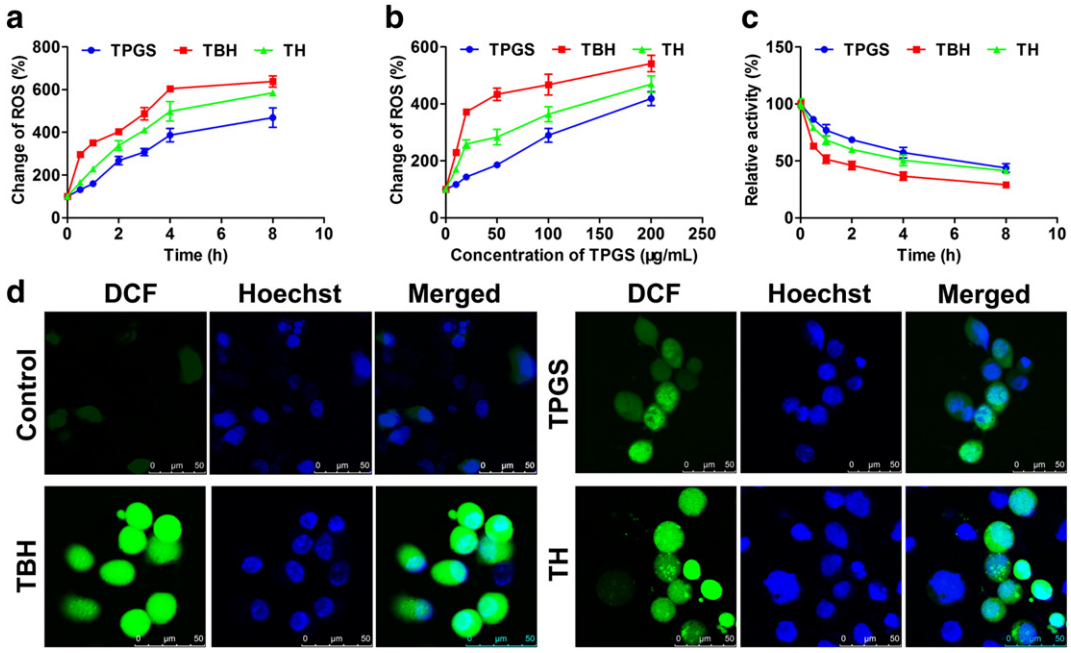

Fig. 2. Detection of amplifying ROS signal in vitro and suppressing the activity of mitochondrial respiratory complex II. (a) The change of ROS level in MCF-7/ADR cells after incubation with TPGS, TBH or TH for different periods of time when comparing with basic ROS level (n = 3). The concentrations of TPGS, TBH and TH were fixed at 200 μg/mL calculated by TPGS. (b) The change of ROS level in MCF-7/ADR cells after incubation with TPGS, TBH or TH for different concentrations of TPGS at 4 h when comparing with basic ROS level (n = 3). (c) The inhibition of TPGS, TBH or TH on the activity of mitochondrial respiratory complex II. (d) Observation of intracellular ROS generation by DCFH-DA staining in MCF-7/ADR cells incubated with DMEM (as control), TPGS, TBH and TH for 4 h. The concentrations of TPGS, TBH and TH were fixed at 200 μg/mL calculated by TPGS. (Green for DCF, blue for Hoechst and scale bar = 50 μm).

nick-end labeling technique (TUNEL) and hematoxylin and eosin staining (H&E) were applied to frozen section tumor samples (drawn at day 14).

2.16. Statistical analysis

Results are given as Mean ± S.D. Statistical significance was tested by two-tailed Student's t-test or one-way ANOVA. Statistical significance was set at $^{*}P < 0.05$ and extreme significance was set at $^{**}P < 0.01$.

3. Results and discussion

3.1. Synthesis and characterization of TBH

TBH synthesis was confirmed by ^{1}H NMR (Fig. S1a) and showed in Fig. 1a. The graft ratio of TPGS (per 100 HA units) linked by arylboronic ester under optimal conditions was 10.9 ± 1.3% (n = 3). In addition, the content of boron determined by ICP-MS was 4.0% in TBH. Both surface tension measurement and the steady-state fluorescence probe technique were applied for determination of critical micelle concentration (CMC). The results revealed that the CMC value of TBH was about 100 μg/mL. To determine the ROS response of TBH in a cancerous microenvironment, GPC was used to evaluate the degradation of TBH in 1 mM H_2O_2. After 4 h, a new peak belonging to TPGS was observed in the chromatogram of TBH (Fig. 1b). This meant that ROS labile arylboronic esters in the TBH were sensitive to H_2O_2-mediated degradation [32]. ^{1}H NMR image of degradation product confirmed that the proton chemical shifts belong to TPGS and arylboronic groups (Fig. S3). Composed of HA and TPGS, another amphiphilic polymer (TH) without ROS sensitivity was synthesized and characterized (Fig. S1b). The similar graft ratio of TPGS (per 100 HA units) and CMC suggested the similar micellization ability and micellar stability toward dilution in vitro and in vivo. In addition, no TPGS peak was observed after first 4 h in GPC due to the lack of sensitivity to ROS microenvironment (Fig. S2).

The quantitative study of ROS triggered TBH degradation revealed that the degradation characteristics of TBH also exhibited time-dependent course. As the incubation time increased to 4 h the degradation ratio of TBH decreased more than 80% and reached a plateau (Fig. 1c).

The DLS results indicated that the change of particle size when TPGS, TBH and TH were treated with H_2O_2, was time- and concentration-dependent. In Fig. 1d, even after 0.25 h incubation, the particle size of TBH remarkably decreased from 42.3 nm to 28.1 nm. As the incubation time increased to 1 h, the particle size of TBH decreased more than 50%, which was similar to the particle size of TPGS. Besides, the concentration-dependent ROS degradation revealed that the particle size of TBH declined with the elevation of concentration of H_2O_2 and reached equilibrium stage when the concentration of H_2O_2 was higher than 0.5 mM after 4 h incubation (Fig. 1e). But little changes in particle size were found for TPGS and TH. The results of GPC and changes in the particle size suggested that an efficient ROS triggered degradation occurred in TBH.

3.2. Amplifying ROS signals in vitro

To demonstrate the capacity of signaling modules to induce ROS regeneration in MCF-7/ADR cells, non-fluorescent DCFH-DA was chosen as ROS marker. After entering into the cell DCFH-DA would be hydrolyzed to DCF and yield a highly green fluorescent signal in the presence of intracellular ROS such as H_2O_2 [33]. Therefore, the fluorescence intensity was found to be proportional to the amount of ROS formed intracellularly. Quantitative analysis found that TBH could rapidly increase the level of ROS in MCF-7/ADR cells (Fig. 2a) due to fast release of TPGS. Even in the initial 0.5 h, the level of ROS increased 3.0-fold for TBH when compared with base ROS level, which was 2.3-fold and 1.8-fold higher than that for TPGS and TH, respectively ($P < 0.05$). TBH micelles also showed stronger ability to heighten ROS level at each concentration point (Fig. 2b). Although TPGS, TBH and TH had the same content of TPGS,

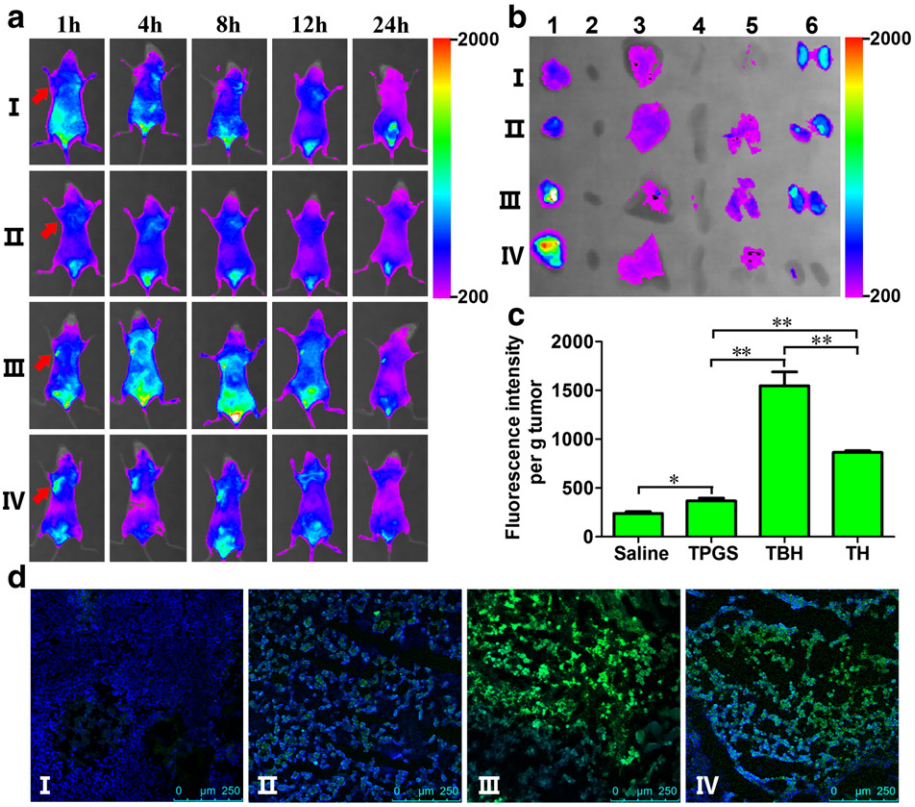

Fig. 3. Ex vivo imaging studies for ROS generation in xenograft MCF-7/ADR tumor-bearing nude mice. (a) Fluorescence images of ROS generation in xenograft MCF-7/ADR tumor-bearing nude mice at 1, 4, 8, 12 and 24 h after intravenous injection of saline (I), TPGS (II), TBH (III) and TH (IV). (b) Fluorescence images of isolated organs separated from MCF-7/ADR tumor-bearing mice in different groups at 24 h. The numeric label for each organ is as follows: 1, tumor; 2, heart; 3, liver; 4, spleen; 5, lung; 6, kidney. (c) Quantitative analysis of fluorescent signals from the tumors and normal tissues (n = 3) $^{*}P < 0.05$, $^{**}P < 0.01$ (two-tailed Student's t-test). (d) CLSM images of ROS generation in tumor tissues in different groups (green for DCF, blue for DAPI in nucleus and scale bars = 250 μm).

difference in ROS generation might be due to the internalization amount of TPGS in cells. Both TBH and TH could be internalized into MCF-7/ADR by CD44 mediated endocytosis with the help of HA [34]. The more the TPGS was internalized into cells the higher the ROS level was. Furthermore, TBH possessed stronger ability of generating ROS than TH did. ROS response of TBH would release TPGS groups quickly, which could induce ROS generation and keep an elevated ROS signal modules in cytoplasm. CLSM results revealed that TBH could induce more strong fluorescence intensity in MCF-7/ADR cells when compared to TPGS and TH, which was similar to the results of quantitative analysis (Fig. 2d).

Next, to confirm the mechanism of ROS intracellular generation in MCF-7/ADR cells, TPGS, TBH or TH was demonstrated to inhibit the

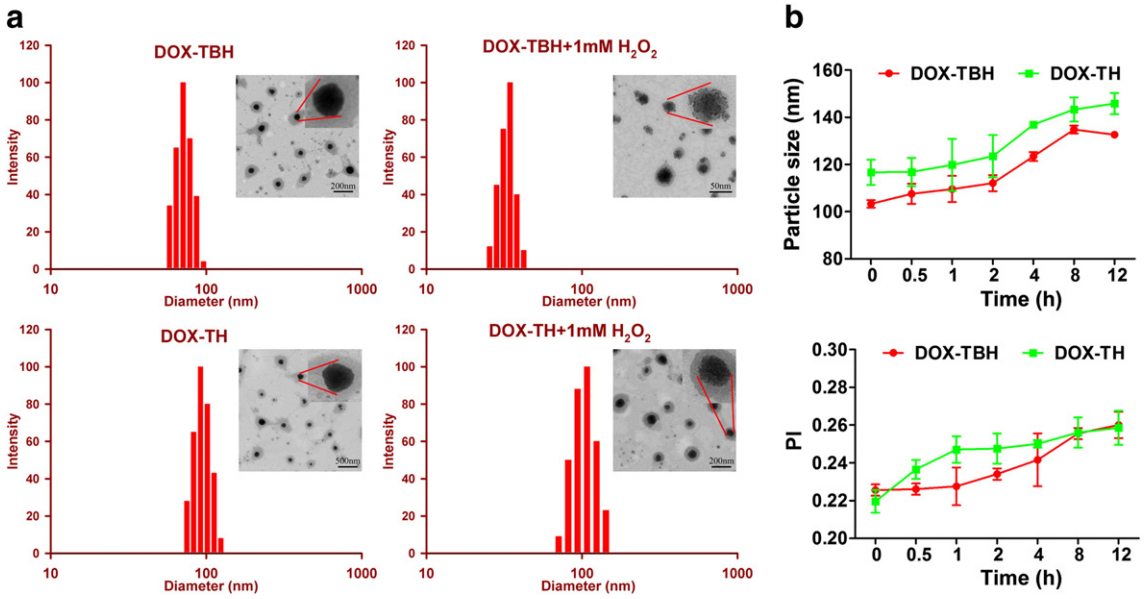

Fig. 4. Preparation and characteristics of DOX-TBH and DOX-TH. (a) Characteristics of DOX-TBH and DOX-TH by DLS and TEM with or without 1 mM H2O2. (b) The stability of DOX-TBH and DOX-TH when incubated with plasma.

activity of mitochondrial respiratory complex II significantly (Fig. 2c), which would cause the electron leak from the respiratory chain to recombine with molecular oxygen to yield ROS [23]. This effect created a kind of intracellular microenvironment with persisting high levels of ROS for TBH degradation, making a cycle of ROS consumption and regeneration with positive feedback, hence, facilitating ROS responsive nanocarrier to deliver efficiently.

3.3. Ex vivo imaging studies for ROS generation in xenograft MCF-7/ADR Tumor-bearing nude mice

Having probed the ROS generating potential of TBH at the cellular level, we next investigated the ability of TBH to generate ROS in the tumor site. The xenograft MCF-7/ADR tumor-bearing nude mice were first injected with free DCFH-DA (2.5 mg/kg) by intratumoral injection, then intravenous injection of saline as control, TPGS, TBH or TH. As showed in Fig. S4, for free DCFH-DA no fluorescence was found without oxidation in vitro. In Fig. 3a, after 1 h post-injection TBH and TH produced tumor-specific fluorescence signal. As time increased, elevated fluorescent signals were found at the tumor site for TBH and TH groups as compared with saline and TPGS groups within 8 h post-injection, highlighting TBH and TH accumulation in tumor by EPR and CD44 mediated active targeting. After 24 h post-injection, tumors as well as normal tissues were harvested for ex vivo imaging. A high level of fluorescence was located in the tumor, while low signals were observed in vital organs (Fig. 3b). The DCF was eliminated mainly by the kidney. For TPGS group, no obvious tumor-specific fluorescence occurred in comparison with TBH and TH groups, suggesting that TPGS could not accumulate in the tumor or internalize by tumor cells effectively because of small molecule size and leaking ability of targeting to tumor. The fluorescence signal of TBH at the tumor site was significantly higher than that of TPGS and TH, which was 4-fold and 2-fold using quantitative analysis, respectively (Fig. 3c). Histopathologic analysis further verified that TBH strongly induced ROS generation and accumulation in tumor cells than TPGS and TH (Fig. 3d).

Giving a thought to safety, in Fig. S5, TBH and TH were non-toxic or low-toxic to normal, i.e. primary brain capillary endothelial cells (BCBCs) and normal hepatocytes (L02). As it was reported previously, due to the generally higher levels of esterase in normal cells such as hepatocytes, colonocytes, fibroblasts or cardiomyocytes, the succinate ester structure of TPGS would be more easily cleaved to produce vitamin E in these tissues [21]. In addition, the biological compatibility evaluation exhibited that no significant difference was found for the blood routine examination after i.v. administration of different materials (Fig. S6a). Both of TBH and TH did not alter the level of IL2, IL6 and INF-λ in serum as well as in spleen, suggesting that TBH and TH did not induce acute inflammation (Fig. S6b). The level of ALT/GPT, AST/GOT and BUN was the same as the saline group, suggesting that no liver and kidney damage occurred after consecutive injection of TBH and TH in healthy mice (Fig. S6c). Moreover, total antioxidant capacity assay revealed that after continuous injection of TBH and TH it still did not change their total antioxidant potential and ROS accumulation was found after treatment in normal tissues, further confirming the biological compatibility of TBH and TH (Fig. S7).

3.4. Preparation and characteristics of DOX-TBH and DOX-TH

Experiments were conducted to demonstrate whether and how the drug delivery nanosystem could help the loaded drug accumulation and retention in MCF-7/ADR cells induced by extra ROS generation and TPGS release after the micelle degradation. DOX-TBH and DOX-TH were prepared by a simple dialysis method. The entrapment efficiencies of DOX-TBH and DOX-TH were 66.35 ± 5.42% and 63.76 ± 6.33% with particle sizes of 83 ± 2.6 nm and 107 ± 3.9 nm and zeta potential of −14.2 ± 1.7 mV and −10.9 ± 0.8 mV, respectively (n = 3). DLS results showed that in the present of 1 mM H_2O_2 the particle size of DOX-TBH sharply decreased; meanwhile, TEM image confirmed that after incubation in 1 mM H_2O_2, the particle size of DOX-TBH changed sharply from 80 nm to 30 nm and the structure became loose and coarse due to ROS labile nature of the DOX-TBH (Fig. 4a). On the other hand, no significant difference was found for DOX-TH when incubated with or without H_2O_2 (Fig. 4a). As mention above, the change of particle size for DOX-TBH was due to the degradation of arylboronic ester in TBH and released TPGS, which would result in smaller particle size.

In addition, in Fig. 4b the stability of DOX-TBH and DOX-TH in plasma revealed that particle size could remain stable during the first 2 h, suggesting that particles could survive in the plasma and prolong blood circulation at first period. According to the "Vroman effect" the plasma protein adsorption was time dependent [35]. Proteins with high concentrations but lower affinity in plasma would initially occupy the surface of the nanoparticles, and then they would be replaced by the proteins with low concentration but higher affinity in plasma, which would cause a rapid and irreversible change of particle size [36]. As the incubation time increases the particle size of DOX-TBH and DOX-TH increases dramatically.

3.5. In vitro drug release of DOX-TBH and DOX-TH

Both DOX-TBH and non-ROS-responsive DOX-TH, which consisted of the same amount of DOX, exhibited a sustained DOX release compared with the DOX solution in saline (Fig. 5a). More importantly, the release rate of DOX-TBH increased observably in the presence of 1 mM H_2O_2, while there was a slight change in the release rate of DOX-TH (Fig. 5b). The faster release might be due to the degradation of arylboronic esters under H_2O_2, which would undergo a triggered disassembly of DOX-TBH leading to expulsion of hydrophobic core (TPGS and DOX). Furthermore, a fast decline in the concentration of H_2O_2 in vitro was observed in the case of DOX-TBH which could be attributed to consumption by oxidative degradation of arylboronic esters. While for free DOX and DOX-TH, the concentration of H_2O_2 decreased slightly over 8 h (Fig. 5c). Besides, the burst release demonstrated by DOX-TBH was dependent on the concentration of H_2O_2 (Fig. 5d). With the increase in concentration of H_2O_2, more DOX-TBH would degrade leading to complete drug release. It can be safely assumed that the disassembly of ROS-triggered nanocarrier is also dependent on the ROS levels in tumor cells, the lower ROS level would result in the hampered degradation of nanocarrier and slower release of cargo. It is obvious that ROS

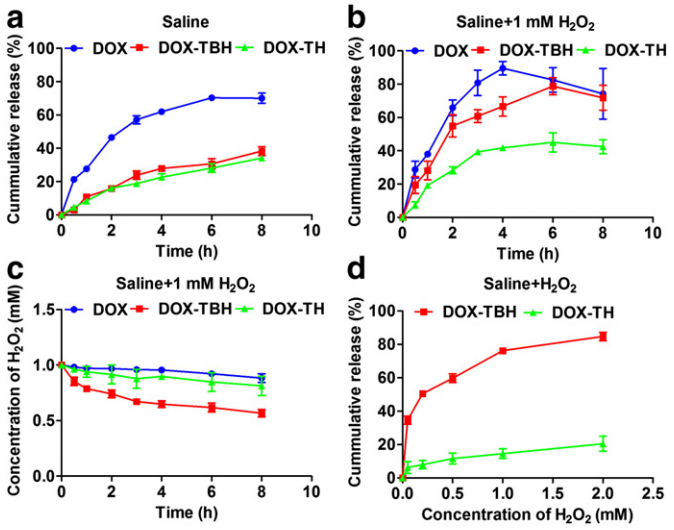

Fig. 5. ROS-triggered DOX release from DOX-TBH and DOX-TH. (a) The release of DOX at 37 °C for free DOX, DOX-TBH and DOX-TH in saline. (b) The release of DOX at 37 °C for free DOX, DOX-TBH and DOX-TH in saline with 1 mM H_2O_2. (c) The change of H_2O_2 concentration in saline with 1 mM H_2O_2. (d) The influence of H_2O_2 concentration on drug release.

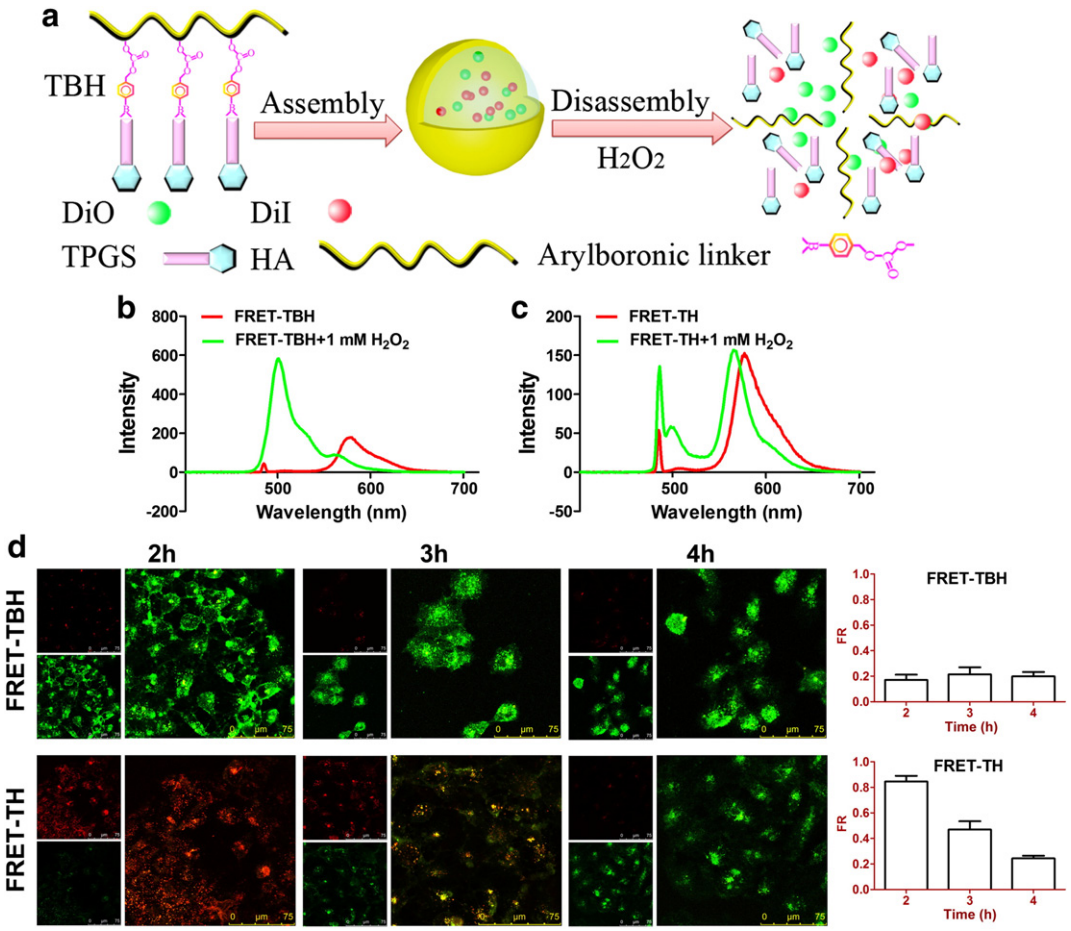

Fig. 6. Intracellular FRET analysis of TBH disassembly. (a) Scheme of FRET-TBH assembly in water and disassembly in 1 mM H_2O_2. (b) Fluorescence emission spectra of FRET-TBH diluted with water (red curve) and 1 mM H_2O_2 (green curve) observed at 484 nm excitation wavelength. (c) Fluorescence emission spectra of FRET-TH diluted with water (red curve) and 1 mM H_2O_2 (green curve) observed at 484 nm excitation wavelength. (d) Confocal images of MCF-7/ADR cells incubated with FRET-TBH and FRET-TH micelles for additional 2, 3 and 4 h. (green for DiO, red for DiI and scale bar = 75 μm).

regeneration in cancer cells would favor the triggered disassembly and subsequent burst delivery of the payload.

3.6. Intracellular ROS-triggered release of TBH

To illustrate the ROS-triggered release of the core-loaded drug in real time in cells, we physically loaded a FRET pair of hydrophobic dyes, DiO as donor and DiI as acceptor, into TBH and TH micelles (referred to as FRET-TBH and FRET-TH) and showed in Fig. 6a. Fluorescence spectra at 484 nm showed that for micelles in deionized water, a strong DiI signal was observed (red curve in Fig. 6b and c) due to the close proximity of DiO and DiI in the micelle core (0–10 nm), with a FRET ratio (FR) of 0.95 and 0.96 for FRET-TBH and FRET-TH, respectively. After decomposition by 1 mM H_2O_2, FRET signal plummeted for FRET-TBH groups and the FR declined from 0.96 to 0.13 during 2 h period (green curve in Fig. 6b), indicating the release of core-loaded probes to medium and disassembly of micelles. On the contrary, the FRET signal decreased gradually for FRET-TH and the FR of FRET-TH was 0.74 after 2 h incubation, which was significantly higher than that of FRET-TBH (green curve in Fig. 6c). These results suggested that FRET pair release from TBH nanocarrier was more sensitive to H_2O_2 than that of TH nanocarrier. The degradation of arylboronic esters triggered by H_2O_2 could be the most likely cause of rapid disassembly of FRET-TBH leading to the release of FRET pair.

CLSM image revealed that FRET signal of FRET-TBH disappeared from MCF-7/ADR cells after an additional 2 h of incubation (Fig. 6d). The fluorescent signal analyzed from the hold cells showed that the FR of FRET-TBH decreased to 0.2 and only DiO signal (green) was observed clearly, indicating that fast release of FRET pair or micelles disassembly occurred intracellularly. Further monitoring FRET signal of FRET-TBH up to 4 h showed a constantly higher disassembly behavior and no significant change was found for the FR from 2 to 4 h. As anticipated for FRET-TH, owing to its poor ROS sensitivity and subsequently delayed disassembly, the reduction of FRET was much slower and weaker as additional incubation time increased from 2 to 4 h (from red to green). With a FR near to 0.2, most of FRET-TH disassembled after an additional 4 h of incubation.

To confirm the ROS-triggered and regenerating mechanism, TPGS was replaced by glycerin monostearate to obtain another ROS-triggered degradation but non-ROS-regenerating amphiphilic materials, named as GBH. GBH synthesis was confirmed by ^{1}H NMR (Fig. S8). After loading FRET pair, the particle size of FRET-GBH was 125 ± 2.8 nm with −16.7 ± 2.1 mV zeta potential. Moreover, as showed in Fig. S9, FRET-GBH was also capable of ROS-triggered release. Fluorescence spectra at 484 nm showed that a remarkable fluorescence switch from DiI to DiO occurred after incubation with 1 mM H_2O_2, suggesting that FRET-GBH was responsive to ROS and the release of FRET pair was dramatically accelerated. Further, the effect of GBH on ROS level in MCF-7/ADR cells revealed that ROS level decreased gradually as the concentration of GBH increased, indicating that the degradation of arylboronic ester in GBH would consume ROS in cytoplasm (Fig. S10a).

As described above, most of FRET-TBH disassembled after additional incubation for 2 h. To illustrate the degradation of ROS triggered release in time course MCF-7/ADR cells were incubated with FRET-TBH and

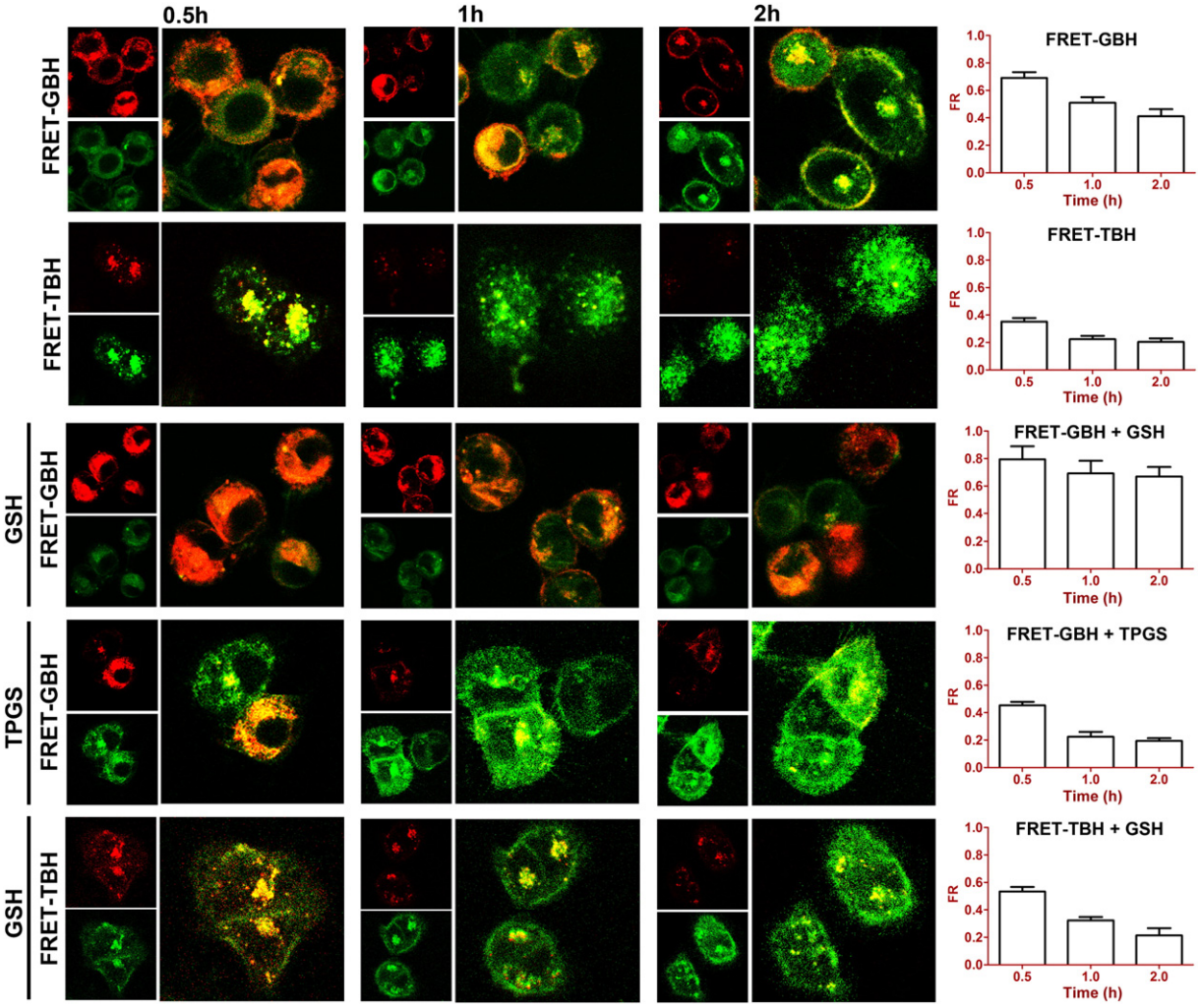

Fig. 7. Study of ROS-triggered and regenerative mechanism. Intracellular disassemble of FRET-GBH, FRET-TBH, FRET-GBH with TPGS, FRET-GBH with GSH and FRET-TBH with GSH on MCF-7/ADR cells after an additional 0.5, 1 and 2 h incubation observed by CLSM (green for DiO, red for DiI and scale bar = 10 μm).

FRET-GBH for 2 h at 37 °C and washed with ice-cold PBS, and subsequently monitored with CLSM after an additional 0.5, 1 and 2 h of incubation. As showed in Fig. 7, both of FRET-TBH and FRET-GBH presented a time-dependent degradation and a decrease of FRET signal was observed inside the cells. The FRET signal in FRET-TBH disappeared more quickly than FRET-GBH and after an additional 0.5 h of incubation FR of FRET-TBH decreased to 0.30, which was 2.3-fold lower than that of FRET-GBH (FR = 0.69, $P < 0.01$), suggesting that ROS regenerating manner of TBH would facilitate the release of cargo modules into cytoplasm. After an additional 1 h of incubation most of FRET-TBH disassembled and the FR remained unchanged for additional 1 to 2 h.

To further confirm the intracellular ROS concentration-dependent release characteristic, co-incubating FRET-GBH with TPGS (200 μg/mL) to elevate intracellular ROS level could dramatically accelerate release of FRET pair from FRET-GBH, which was comparable to that of FRET-TBH. In contrast, for additional 2 h incubation no remarkable release of FRET pair was observed by inhibiting intracellular ROS level with glutathione (GSH, 500 μg/mL), an antioxidant and free radicals scavenger [37] (Fig. S10b), further demonstrating intracellular ROS concentration-dependent drug release of ROS-triggered drug delivery nanosystem. Interestingly, as TBH could efficiently induce ROS generation, the inhibitory effect of GSH to FRET-TBH was much weaker than that to FRET-GBH. Most of FRET pair release from FRET-TBH for additional 2 h incubation. As it was reported, redox property changes during cancer development and disease progression [15]. In this study, TBH could create a kind of ROS positive feedback microenvironment with persisting high levels of ROS generation necessary for degradation of ROS-triggered nanosystem no matter on reduced or oxidized intracellular microenvironment.

3.7. Enhanced accumulation, retention, cytotoxicity and apoptosis of DOX in MCF-7/ADR cells by DOX-TBH

In time-dependent uptake study, owing to the efflux of DOX by P-gp, the uptake index (UI) of free DOX in MCF-7/ADR cells was only 0.803 ± 0.085 μg per mg protein after 4 h of incubation. Incubation with DOX-TBH and DOX-TH for 4 h, the UI in MCF-7/ADR cells significantly increased, which reached up to 11-fold and 7-fold higher than that of free DOX, respectively (Fig. 8a). Except for free DOX, the uptake of DOX presented concentration-dependent and reached a plateau at 20 μg/mL of DOX (Fig. 8b). Compared with DOX-TH, DOX-TBH revealed higher UI, indicating that ROS-triggered DOX-TBH was an effective intracellular nanocarrier delivery system for overcoming MDR.

In another experiment, we determined how DOX was retained in cells. A fast decline in intracellular DOX level was observed in MCF-7/ADR cells pre-incubated with free DOX as a result of drug efflux by P-gp, only 19.67 ± 4.69% DOX was retained in the cells after 4 h (Fig. 8c). However, the amount and the efflux rate of DOX were significantly lower when pre-incubated with DOX-TBH and DOX-TH. The remarkable retention effect for DOX-TBH was noticed when compared

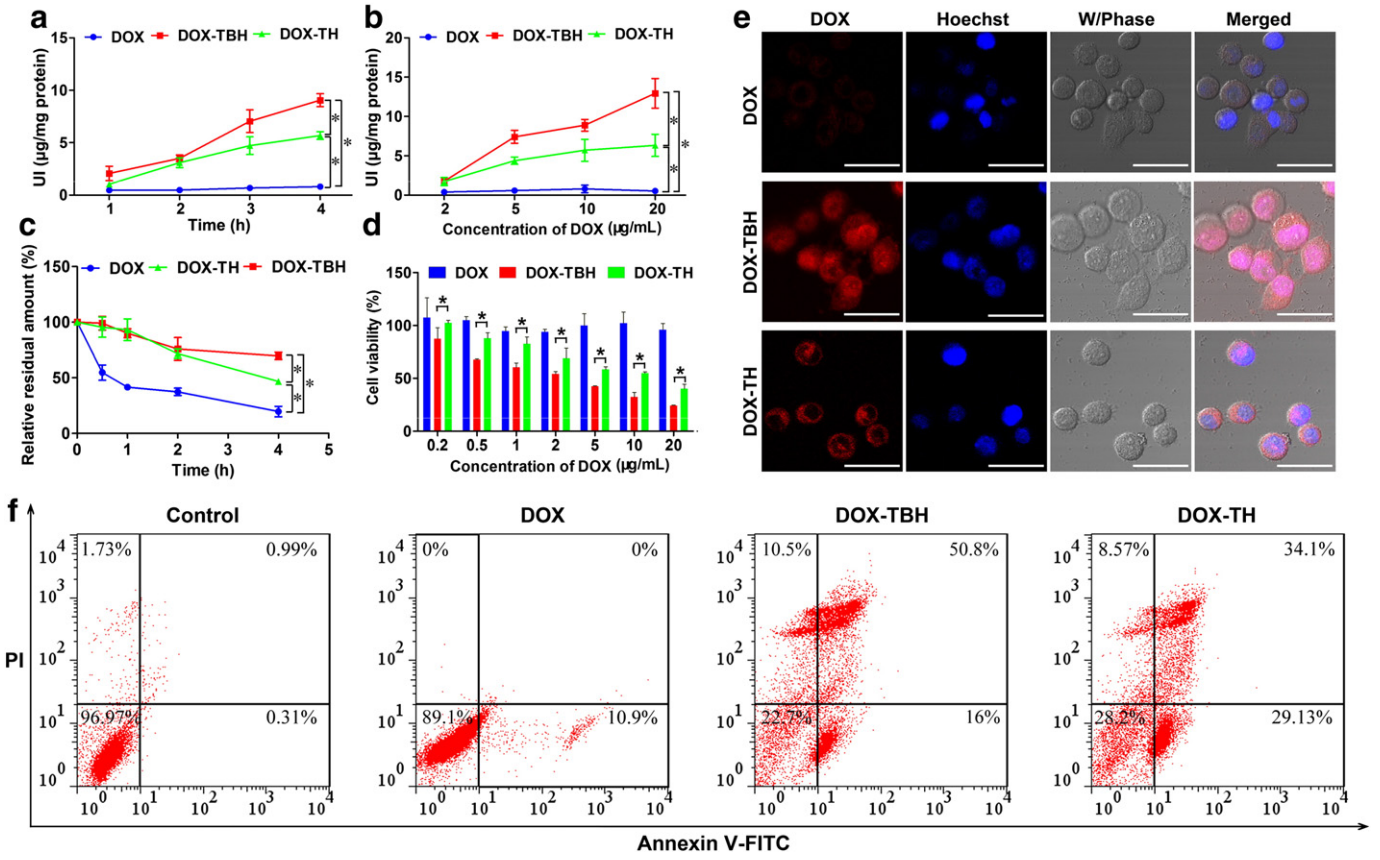

Fig. 8. Enhanced accumulation, retention, cytotoxicity and apoptosis of DOX in MCF-7/ADR cells by DOX-TBH. (a) The influence of concentration of DOX on intracellular uptake in MCF-7/ADR cells. (b) The influence of time on intracellular uptake in MCF-7/ADR cells. (c) Retention of DOX in MCF 7/ADR cells after pre-incubation with free DOX, DOX-TBH or DOX-TH for 4 h (The concentration of total DOX in the free DOX pre-incubation was 40 μg/mL, while it was 10 μg/mL for DOX-TBH and DOX-TH). (d) Cell survival of MCF-7/ADR cells after chemotherapy for 24 h. (e) CLSM study of MCF-7/ADR cells incubated with free DOX, DOX-TBH and DOX-TH (The concentration of DOX was 10 μg/mL; scale bar = 50 μm). (f) Flow cytometric analysis of MCF-7/ADR cells apoptosis induced by free DOX, DOX-TBH or DOX-TH for 12 h using the Annexin V-FITC/PI staining (The concentration of DOX was 10 μg/mL). $^{*}P < 0.05$; $^{**}P < 0.01$.

with DOX-TH (69.72 ± 3.29% vs 46.75 ± 1.79%, $P < 0.05$) after 4 h of incubation. As over-expression of the drug efflux transporters is relevant to the major type of drug resistance in tumor cells, the property to evade and preferably inhibit drug pump efflux activity has been expected to overcome MDR [38]. TPGS exhibits concentration-dependent inhibition of efflux pump ATPase without inducing significant ATPase activity on its own [39]. As demonstrated above, DOX-TBH in MCF-7/ADR cells could quickly degrade, suggesting that more amounts of TPGS would dissociate into cytoplasm, which would function more quickly and effectively than DOX-TH to hinder DOX efflux. A site-dependent drug release character is also vital for drug molecules to reach their target, leading to higher intracellular drug concentration necessary for therapeutic efficacy [40].

Furthermore, qualitative analysis by CLSM indicated that faint red fluorescence signals in cytoplasm region were observed for free DOX after 4 h incubation (Fig. 8e) due to efflux by P-gp. Similar to the quantitative analysis strong fluorescence signals were observed in MCF-7/ADR cells when incubated with DOX-TBH and DOX-TH. For DOX-TH the fluorescence signals dispersed in the peri-nuclear region. It must be mentioned that DOX-TH did not have the ROS responsive DOX release characteristic and the insufficient intracellular drug release remained rate-limiting steps for reaching the therapeutic drug concentration level in nuclei. More importantly, with the function of ROS-triggered release and ROS regeneration, the released DOX from DOX-TBH quickly accumulated into the nuclei, suggesting that enhanced cytotoxicity would be occurred when comparing to DOX-TH.

Furthermore, to confirm the enhanced cytotoxicity and apoptosis by effectively releasing DOX from DOX-TBH, MTT assay was first used to evaluate the cytotoxicity in MCF-7/ADR cells. In the research scope free DOX did not affect the cell viability. But, treatment of DOX-TBH exhibited elevated cytotoxicity when compared with DOX-TH in MCF-7/ADR cells ($IC_{50} = 2.75 \pm 0.4$ μg/mL for DOX-TBH and $IC_{50} = 10.39 \pm 1.91$ μg/mL for DOX-TH, $P < 0.05$) (Fig. 8d). This approves the supremacy of continuous ROS-triggered DOX release over conventional drug delivery approaches in resistant cancer cells. Annexin V-FITC/PI detection was conducted to compare the apoptosis-inducing effect of DOX-TBH and DOX-TH. According to the mechanisms of Annexin V-FITC/PI detection, cells under initiation of apoptosis would be stained by Annexin V-FITC while late apoptotic cells would be labeled by PI. In Fig. 8f, both DOX-TBH and DOX-TH had similar total apoptotic ratio (66.8% of DOX-TBH vs 63.2% of DOX-TH). While compose of apoptotic ratio revealed that DOX-TBH could induce much more late apoptosis in comparison with DOX-TH (50.8% vs 34.1%, $P < 0.05$), further verifying the enhanced cytotoxicity and apoptosis-inducing activity of ROS-triggered and regenerating nanosystem in resistant cancer cells.

3.8. In vivo biodistribution and therapeutic efficacy

To verify the feasibility of DOX-TBH and DOX-TH for cancer therapy in vivo, the biodistribution and antitumor efficacy were estimated in xenograft MCF-7/ADR cells tumor-bearing mice. DiR, a near infrared dye, was loaded into TBH and TH micelles (DiR-TBH and DiR-TH) and the in vivo biodistribution at specific time points was recorded with NIR imaging system (Fig. 9a). It could be seen from the fluorescence intensity in tumors after 24 h post-injection that DiR-TBH exhibited stronger tumor targeting, judging from 5.41-fold higher than DiR-TH

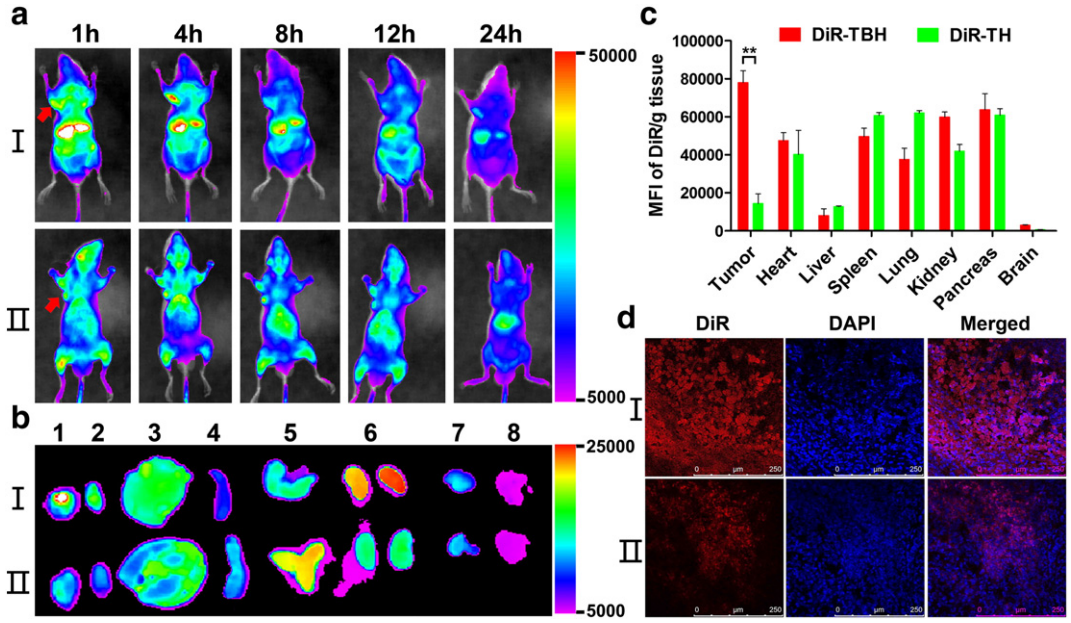

Fig. 9. In vivo tumor-targeting of DiR-TBH and DiR-TH. (a) In vivo fluorescence imaging of the xenograft MCF-7/ADR tumor-bearing nude mice at 1, 4, 8, 12 and 24 h after intravenous injection of DiR-TBH (I) and DiR-TH (II). (b) Ex vivo fluorescence imaging of tumor and tissues harvested from the xenograft MCF-7/ADR tumor-bearing nude mice at 24 h post-injection. The numeric label for each organ is as follows: 1, tumor; 2, heart; 3, liver; 4, spleen; 5, lung; 6, kidney; 7, pancreas; 8, brain. (c) Semi-quantification of DiR-TBH and DiR-TH in the isolated tumor and tissues of xenograft MCF-7/ADR tumor-bearing nude mice (n = 3). (d). CLSM images of DiR in tumor tissues in different groups (red = DiR in MCF-7/ADR cells; blue = cell nucleus stained by DAPI; scale bar = 250 μm). $^{**}P < 0.01$.

in tumor site (Fig. 9b and c). Histopathological analysis of tumor tissues by CLSM also indicated similar results to quantitative analysis (Fig. 9d). TBH and TH possessed the potential for efficiently inducing ROS generation in tumor tissue. The amplified drug delivery by TBH could be ascribed to the augmented ROS signal which would favor the degradation of ROS-triggered nanomaterial to inhibit MDR tumor cells efflux and enhance drug retention. All the in vitro and in vivo results suggested the significance of ROS triggered and regenerating mechanism of this novel ROS sensitive system.

Moreover, the in vivo biodistribution of DOX solution, DOX-TBH and DOX-TH after intravenous administration was also evaluated by quantitatively detecting the DOX amounts in different tissues. Both TBH and TH micelles exhibited the same pharmacokinetic behavior and an enhanced blood circulation compared to the free DOX (Fig. 10a), which suggested that higher concentrations of DOX for DOX-TBH and DOX-TH would remain in the systemic circulation for improving therapeutic index and accumulate in solid tumors through enhanced permeability and retention (EPR) effect. In addition, DOX-TBH exhibited higher DOX accumulation in the tumor than the DOX solution and DOX-TH. The DOX amount in the tumor tissues delivered by DOX-TBH was 5.3 and 2.1 fold higher than that of those delivered by the DOX solution and DOX-TH, respectively, at 4 h post-injection. According to Table S1, the $AUC_{0\sim t}$ of DOX-TBH in tumor showed 4.3-fold and 2.1-fold higher than that of DOX solution and DOX-TH. Hence, it was proved that DOX-TBH had higher tumor targeting potential because of both passive and active targeting mechanisms.

No evident difference was found in the tumor volumes after successive intravenous administration of free DOX due to MDR. However, the efficiency of DOX-TBH and DOX-TH for cancer therapy showed that DOX-TBH and DOX-TH significantly reduced the tumor volumes when compared to the free DOX (Fig. 10b). Moreover, DOX-TBH displayed a prominent effect on tumor-size reduction and delivered the more distinguishable effect by extending the survival period of the tumor bearing mice when compared to DOX-TH (Fig. 10c), suggesting that the efficient intracellular delivery and incessant ROS-triggered and regenerating nanosystem were of great importance to enhanced antitumor activity. No notable change in body weights of the mice during the treatment was found for DOX-TBH in comparison with the saline group (Fig. 10d). Tumor tissues' histological TUNEL analysis of different treatment groups also revealed that no obvious apoptosis was found in tumors of control group (apoptosis ratio < 5%) (Fig. 10e and f). However, markedly increased percentage of apoptotic and necrotic tumor cells was observed in treatment groups especially for DOX-TBH groups; nearly 90% of tumor cells underwent apoptosis or necrosis while the apoptosis ratio of DOX-TH and DOX was only 50% and 18%, respectively (Fig. 10f). In addition, the histologic images using H&E staining showed that treatment with DOX-TBH, a massive cancer cell underwent necrosis in the tumor site (Fig. 10e) while no significant pathological abnormalities in the heart, liver, spleen, lung and kidney were observed (Fig. S11). These results verified that due to ROS responsiveness and regeneration attribute of DOX-TBH a high therapeutic effect on drug resistant human breast cancer could be expected.

4. Conclusion

In summary, we developed a novel targeted drug delivery nanosystem based on TPGS, arylboronic esters and HA for anticancer drug delivery, which was not only responding to ROS signal for drug release but also self-regenerating ROS signal in cytoplasm, simultaneously. Our results suggested that EPR effect and targeting moiety do help the formulations to concentrate into the tumor cells; nonetheless, adequate drug release in the tumors also has a significant role in the success of therapy. We achieved this goal by developing a ROS-triggered and regenerating nanosystem that keeps high levels of ROS in tumor microenvironment, rapidly releasing drug and retaining it effectively to overcome the drug resistance of tumor.

Acknowledgments

This work was supported by the National Natural Science Foundation of China (No.81273467), the Fundamental Research Funds for the Central Universities (JKY2011072) and the National Basic Research Program of China (2015CB755500).

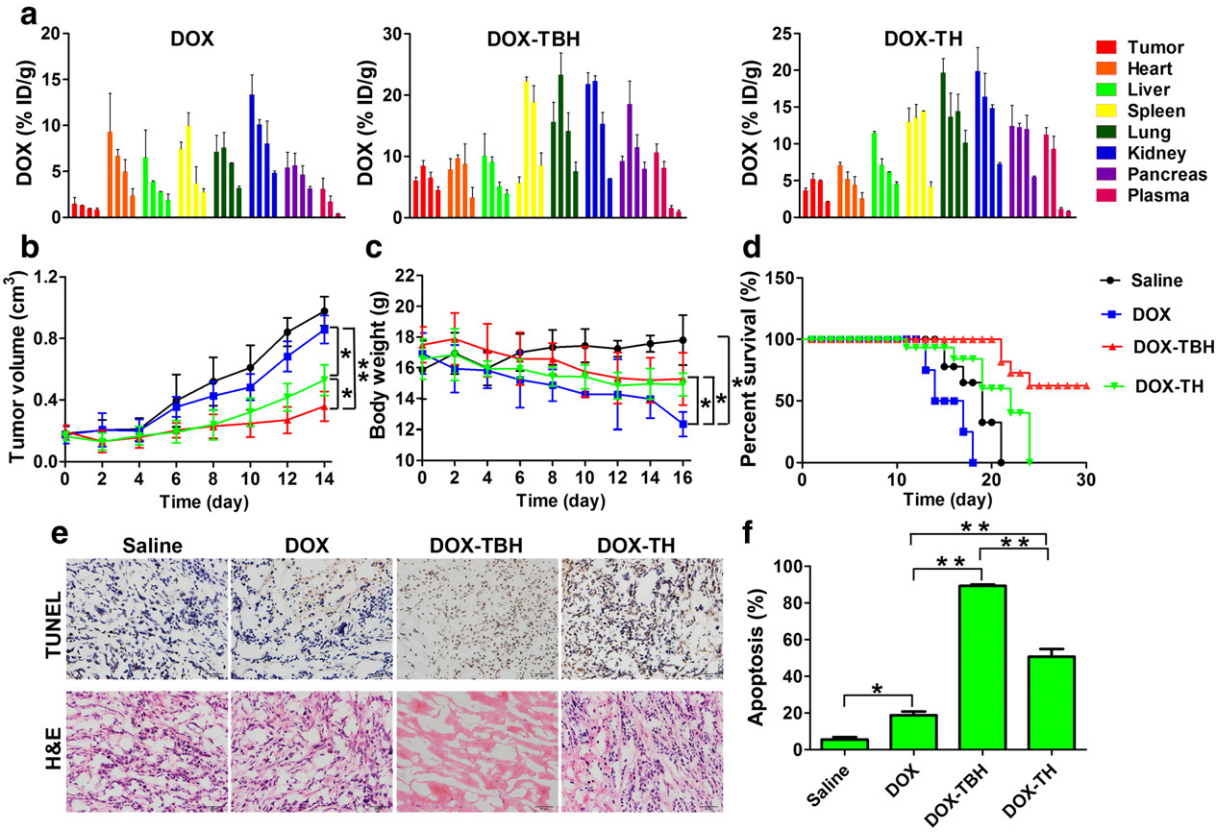

Fig. 10. Tumor targetability and antitumor activity. (a) Biodistribution profiles of DOX accumulation in the plasma, heart, liver, spleen, lung, kidney, pancreas and tumor of the xenograft MCF-7/ADR tumor-bearing nude mice following intravenous injection of the DOX solution, DOX-TBH and DOX-TH at a DOX dose of 2 mg/kg for 0.5, 4, 12 and 24 h. DOX/Tissue (% ID/g) is the ratio of the DOX amount in different tissues to the total injected dose. (b) Xenograft MCF-7/ADR tumor growth curves of different groups after treatments. (c) The body weight variation of xenograft MCF-7/ADR tumor-bearing nude mice during treatment. (d) Survival rates of xenograft MCF-7/ADR tumor-bearing nude mice after treatments. (e) Histological study of tumor tissues after treatment by TUNEL assay and hematoxylin and eosin staining. (f) The percentage of apoptotic cells after treatment (n = 3). $^{*}P < 0.05$ and $^{**}P < 0.01$.

Appendix A. Supplementary data

Supplementary data to this article can be found online at http://dx.doi.org/10.1016/j.jconrel.2014.09.020.

References

[1] Q. Yin, J. Shen, Z. Zhang, H. Yu, Y. Li, Reversal of multidrug resistance by stimuli-responsive drug delivery systems for therapy of tumor, Adv. Drug Deliv. Rev. 65 (2013) 1699–1715.
[2] S. Kunjachan, B. Rychlik, G. Storm, F. Kiessling, T. Lammers, Multidrug resistance: physiological principles and nanomedical solutions, Adv. Drug Deliv. Rev. 65 (2013) 1852–1865.
[3] T. Minko, L. Rodriguez-Rodriguez, V. Pozharov, Nanotechnology approaches for personalized treatment of multidrug resistant cancers, Adv. Drug Deliv. Rev. 65 (2013) 1880–1895.
[4] A.R. Kirtane, S.M. Kalscheuer, J. Panyam, Exploiting nanotechnology to overcome tumor drug resistance: challenges and opportunities, Adv. Drug Deliv. Rev. 65 (2013) 1731–1747.
[5] F. Wang, Y.C. Wang, S. Dou, M.H. Xiong, T.M. Sun, J. Wang, Doxorubicin-tethered responsive gold nanoparticles facilitate intracellular drug delivery for overcoming multidrug resistance in cancer cells, ACS Nano 5 (2011) 3679–3692.
[6] Y.J. Lee, R. Graeser, F. Kratz, K.E. Geckeler, Paclitaxel-loaded polymer nanoparticles for the reversal of multidrug resistance in breast cancer cells, Adv. Funct. Mater. 21 (2011) 4211–4218.
[7] Y.C. Wang, F. Wang, T.M. Sun, J. Wang, Redox-responsive nanoparticles from the single disulfide bond-bridged block copolymer as drug carriers for overcoming multidrug resistance in cancer cells, Bioconjug. Chem. 22 (2011) 1939–1945.
[8] R. Yamada, M.B. Kostova, R.K. Anchoori, S. Xu, N. Neamati, S.R. Khan, Biological evaluation of paclitaxel-peptide conjugates as a model for MMP2-targeted drug delivery, Cancer Biol. Ther. 9 (2010) 192–203.
[9] Q. Jiang, C. Song, J. Nangreave, X. Liu, L. Lin, D. Qiu, Z.G. Wang, G. Zou, X. Liang, H. Yan, B. Ding, DNA origami as a carrier for circumvention of drug resistance, J. Am. Chem. Soc. 134 (2012) 13396–133403.
[10] K. Liang, G.K. Such, Z. Zhu, S.J. Dodds, A.P. Johnston, J. Cui, H. Ejima, F. Caruso, Engineering cellular degradation of multilayered capsules through controlled cross-linking, ACS Nano 6 (2012) 10186–10194.
[11] J. Lai, B.P. Shah, E. Garfunkel, K.B. Lee, Versatile fluorescence resonance energy transfer-based mesoporous silica nanoparticles for real-time monitoring of drug release, ACS Nano 7 (2013) 2741–2750.
[12] Z. Luo, K. Cai, Y. Hu, J. Li, X. Ding, B. Zhang, D. Xu, W. Yang, P. Liu, Redox-responsive molecular nanoreservoirs for controlled intracellular anticancer drug delivery based on magnetic nanoparticles, Adv. Mater. 24 (2012) 431–435.
[13] H. Kim, S. Kim, C. Park, H. Lee, H.J. Park, C. Kim, Glutathione-induced intracellular release of guests from mesoporous silica nanocontainers with cyclodextrin gatekeepers, Adv. Mater. 22 (2010) 4280–4283.
[14] A. Albini, M.B. Sporn, The tumour microenvironment as a target for chemoprevention, Nat. Rev. Cancer 7 (2007) 139–147.
[15] P.D. Ray, B.W. Huang, Y. Tsuji, Reactive oxygen species (ROS) homeostasis and redox regulation in cellular signaling, Cell. Signal. 24 (2012) 981–990.
[16] J. Wang, X. Sun, W. Mao, W. Sun, J. Tang, M. Sui, Y. Shen, Z. Gu, Tumor redox heterogeneity-responsive prodrug nanocapsules for cancer chemotherapy, Adv. Mater. 25 (2013) 3670–3676.
[17] S. Wadhwa, R.J. Mumper, Polypeptide conjugates of D-penicillamine and idarubicin for anticancer therapy, J. Control. Release 158 (2012) 215–223.
[18] M.H. Xiong, Y. Bao, X.J. Du, Z.B. Tan, Q. Jiang, H.X. Wang, Y.H. Zhu, J. Wang, Differential anticancer drug delivery with a nanogel sensitive to bacteria-accumulated tumor artificial environment, ACS Nano 7 (2013) 10636–10645.
[19] V.M. Geoffrey, H.P. Ji, Y.L. Kevin, S. Neetu, S. Christian, M. Rolf, E.B. Wolfgang, R. Erkki, J.S. Michael, N.B. Sangeeta, Nanoparticles that communicate in vivo to amplify tumour targeting, Nat. Mater. 10 (2011) 545–552.
[20] E.M. Collnot, C. Baldes, M.F. Wempe, R. Kappl, J. Huttermann, J.A. Hyatt, K.J. Edgar, U.F. Schaefer, C.M. Lehr, Mechanism of inhibition of P-glycoprotein mediated efflux by vitamin E TPGS: influence on ATPase activity and membrane fluidity, Mol. Pharm. 4 (2007) 465–474.
[21] J. Neuzil, T. Weber, N. Gellert, C. Weber, Selective cancer cell killing by alpha-tocopheryl succinate, Br. J. Cancer 84 (2001) 87–89.
[22] H.J. Youk, E. Lee, M.K. Choi, Y.J. Lee, J.H. Chung, S.H. Kim, C.H. Lee, S.J. Lim, Enhanced anticancer efficacy of alpha-tocopheryl succinate by conjugation with polyethylene glycol, J. Control. Release 107 (2005) 43–52.

[23] L.F. Dong, P. Low, J.C. Dyason, X.F. Wang, L. Prochazka, P.K. Witting, R. Freeman, E. Swettenham, K. Valis, J. Liu, R. Zobalova, J. Turanek, D.R. Spitz, F.E. Domann, I.E. Scheffler, S.J. Ralph, J. Neuzil, Alpha-tocopheryl succinate induces apoptosis by targeting ubiquinone-binding sites in mitochondrial respiratory complex II, Oncogene 27 (2008) 4324–4335.
[24] A.R. Lippert, G.C. Van de Bittner, C.J. Chang, Boronate oxidation as a bioorthogonal reaction approach for studying the chemistry of hydrogen peroxide in living systems, Acc. Chem. Res. 44 (2011) 793–804.
[25] J.A. Burdick, G.D. Prestwich, Hyaluronic acid hydrogels for biomedical applications, Adv. Mater. 23 (2011) 41–56.
[26] M. Han, Q. Lv, X.J. Tang, Y.L. Hu, D.H. Xu, F.Z. Li, W.Q. Liang, J.Q. Gao, Overcoming drug resistance of MCF-7/ADR cells by altering intracellular distribution of doxorubicin via MVP knockdown with a novel siRNA polyamidoamine–hyaluronic acid complex, J. Control. Release 163 (2012) 136–144.
[27] M.T. Peracchia, C. Vauthier, C. Passirani, P. Couvreur, D. Labarre, Complement consumption by poly(ethylene glycol) in different conformations chemically coupled to poly(isobutyl 2-cyanoacrylate) nanoparticles, Life Sci. 61 (1997) 749–761.
[28] C.A. Gay, J.M. Gebicki, Perchloric acid enhances sensitivity and reproducibility of the ferric-xylenol orange peroxide assay, Anal. Biochem. 304 (2002) 42–46.
[29] H. Chen, S. Kim, L. Li, S. Wang, K. Park, J.X. Cheng, Release of hydrophobic molecules from polymer micelles into cell membranes revealed by Forster resonance energy transfer imaging, Proc. Natl. Acad. Sci. U. S. A. 105 (2008) 6596–6601.
[30] S. Zhao, W. Dai, B. He, J. Wang, Z. He, X. Zhang, Q. Zhang, Monitoring the transport of polymeric micelles across MDCK cell monolayer and exploring related mechanisms, J. Control. Release 158 (2012) 413–423.
[31] Y. Xu, X.F. Jin, Q.N. Ping, J. Cheng, M.J. Sun, F. Cao, W.L. You, D.F. Yuan, A novel lipoprotein-mimic nanocarrier composed of the modified protein and lipid for tumor cell targeting delivery, J. Control. Release 146 (2010) 299–308.
[32] K.E. Broaders, S. Grandhe, J.M. Frechet, A biocompatible oxidation-triggered carrier polymer with potential in therapeutics, J. Am. Chem. Soc. 133 (2011) 756–758.
[33] Y. Cui, Y. Zhao, Y. Tian, W. Zhang, X. Lu, X. Jiang, The molecular mechanism of action of bactericidal gold nanoparticles on *Escherichia coli*, Biomaterials 33 (2012) 2327–2333.
[34] J.H. Park, H.J. Cho, H.Y. Yoon, I.S. Yoon, S.H. Ko, J.S. Shim, J.H. Cho, K. Kim, I.C. Kwon, D.D. Kim, Hyaluronic acid derivative-coated nanohybrid liposomes for cancer imaging and drug delivery, J. Control. Release 174 (2014) 98–108.
[35] S. Harnisch, R.H. Muller, Adsorption kinetics of plasma proteins on oil-in-water emulsions for parenteral nutrition, Eur. J. Pharm. Biopharm. 49 (2000) 41–46.
[36] Z.G. Su, J.X. Niu, Y.Y. Xiao, Q.N. Ping, M.J. Sun, A.W. Huang, W.L. You, X.Y. Sang, D.F. Yuan, Effect of octreotide-polyethylene glycol(100) monostearate modification on the pharmacokinetics and cellular uptake of nanostructured lipid carrier loaded with hydroxycamptothecine, Mol. Pharm. 8 (2011) 1641–1651.
[37] R. Cascella, E. Evangelisti, M. Zampagni, M. Becatti, G. D'Adamio, A. Goti, G. Liguri, C. Fiorillo, C. Cecchi, S-linolenoyl glutathione intake extends life-span and stress resistance via Sir-2.1 upregulation in *Caenorhabditis elegans*, Free Radic. Biol. Med. 73C (2014) 127–135.
[38] B. Al-Lazikani, U. Banerji, P. Workman, Combinatorial drug therapy for cancer in the post-genomic era, Nat. Biotechnol. 30 (2012) 679–692.
[39] E.M. Collnot, C. Baldes, U.F. Schaefer, K.J. Edgar, M.F. Wempe, C.M. Lehr, Vitamin E TPGS P-glycoprotein inhibition mechanism: influence on conformational flexibility, intracellular ATP levels, and role of time and site of access, Mol. Pharm. 7 (2010) 642–651.
[40] S. Febvay, D.M. Marini, A.M. Belcher, D.E. Clapham, Targeted cytosolic delivery of cell-impermeable compounds by nanoparticle-mediated, light-triggered endosome disruption, Nano Lett. 10 (2010) 2211–2219.